

REPORT DOCUMENTATION PAGE			Form Approved OMB No 0704-0188		
The public reporting burden for this collection of information is estimated to average 1 hour per response, including the time for reviewing instructions, searching existing data sources, gathering and maintaining the data needed, and completing and reviewing the collection of information. Send comments regarding this burden estimate or any other aspect of this collection of information, including suggestions for reducing the burden, to the Department of Defense, Executive Service Directorate (0704-0188). Respondents should be aware that notwithstanding any other provision of law, no person shall be subject to any penalty for failing to comply with a collection of information if it does not display a currently valid OMB control number.					
PLEASE DO NOT RETURN YOUR FORM TO THE ABOVE ORGANIZATION.					
1. REPORT DATE (DD-MM-YYYY) 12-12-2017		2. REPORT TYPE FINAL		3. DATES COVERED (From - To) 06/01/2014-07/31/2017	
4. TITLE AND SUBTITLE Scaling up complexity of DNA brick structures			5a. CONTRACT NUMBER		
			5b. GRANT NUMBER N00014-16-1-2182/N00014-14-1-0610		
			5c. PROGRAM ELEMENT NUMBER		
6. AUTHOR(S) Peng Yin			5d. PROJECT NUMBER		
			5e. TASK NUMBER		
			5f. WORK UNIT NUMBER		
7. PERFORMING ORGANIZATION NAME(S) AND ADDRESS(ES) Harvard Medical School 25 Shattuck Street, Suite 509 Boston, MA 02115-6027			8. PERFORMING ORGANIZATION REPORT NUMBER 167896		
9. SPONSORING/MONITORING AGENCY NAME(S) AND ADDRESS(ES) ONR REG BCSTON N62879 495 SUMMER STREET ROOM 627 BOSTON, MA 02210-2109			10. SPONSOR/MONITOR'S ACRONYM(S) ONR		
			11. SPONSOR/MONITOR'S REPORT NUMBER(S) N62879		
12. DISTRIBUTION/AVAILABILITY STATEMENT Approved for Public Release; distribution is Unlimited					
13. SUPPLEMENTARY NOTES					
14. ABSTRACT DNA-based assemblies of increasing complexity may allow for novel applications in vitro and in vivo. Here, we increase the number of unique, addressable components in "DNA Brick" structures by 100-fold, from hundreds to 10,000 – for a molecular weight of 1 CDa. We also create relatively flat, micron-scale structures from these bricks using a repeating crystal approach, and apply the results to patterning carbon nanotubes for the electronics industry to help meet ever-increasing speed and efficiency targets. Further, we also develop single-stranded DNA and RNA Origami approaches, which allow for rapid copying and robust assembly of large structures. Finally, we develop in vivo structures capable of controlling RNA translation with levels of precision not yet seen in synthetic biology, and combine orthogonal signal control to execute complex logical functions.					
15. SUBJECT TERMS DNA nanotechnology, self-assembly, nanostructures, carbon nanotubes, translational regulation, synthetic biology					
16. SECURITY CLASSIFICATION OF:			17. LIMITATION OF ABSTRACT	18. NUMBER OF PAGES	19a. NAME OF RESPONSIBLE PERSON
a. REPORT	b. ABSTRACT	c. THIS PAGE			Peng Yin
U	U	U	UU	22	19b. TELEPHONE NUMBER (Include area code) 617-432-7731

Final Report for N00014-14-1-0610 & N00014-16-1-2182

Scaling up complexity of DNA brick structures

Principle Investigator: Peng Yin, Harvard University

Table of Contents

1	Heading	3
2	Scientific and Technical Objectives	3
3	Approach	3
4	Concise Accomplishments	3
5	Expanded Accomplishments	4
5.1	Novel structure generation, expansion, and application	4
5.1.1	High-precision scaling of ultra-dense carbon nanotube arrays at 2-nm resolution	4
5.1.2	Single-stranded DNA and RNA Origami.	4
5.1.3	Programmable Self-Assembly of Three-Dimensional Nanostructures from 10,000 Unique Components.	5
5.1.4	DNA nanostructures-mediated molecular imprinting lithography.....	5
5.1.5	Programmably-shaped carbon nanostructure from shape-conserving carbonization of DNA.....	5
5.1.6	A compact DNA cube with side length 10 nm.....	6
5.1.7	Casting inorganic structures with DNA molds.	6
5.1.8	DNA brick crystals with prescribed depths.	6
5.2	DNA-based synthetic biology	6
5.2.1	Programmable autonomous synthesis of single-stranded DNA.....	6
5.2.2	A DNA nanoscope via auto-cycling proximity recording.....	7
5.2.3	Complex cellular logic computation using ribocomputing devices.	7
5.2.4	DyNAMiC Workbench: an integrated development environment for dynamic DNA nanotechnology.....	7
5.2.5	Toehold switches: de-novo-designed regulators of gene expression.	8
5.3	Imaging technologies and applications	8
5.3.1	Rapid sequential in situ multiplexing with DNA-Exchange-Imaging in Neuronal Cells and Tissues.....	8
5.3.2	DNA-barcoded labeling probes for highly multiplexed Exchange-PAINT imaging.....	8
5.3.3	Polyhedra self-assembled from DNA tripods and characterized with 3D DNA-PAINT.	9
6	Major problems / Issues	9
7	Technology Transfer	9
8	Foreign Collaborations and Supported Foreign Nationals	9
9	Productivity	9
9.1	Refereed Journal Articles	9
9.1.1	Structures.....	9
9.1.2	Synthetic Biology.....	10

9.1.3	Imaging.....	10
9.2	Non-Refereed Journal Articles	10
9.3	Workshops and Conferences.....	10
9.4	Translation: Patents	12
9.5	Translation: Start-ups	13
9.6	Awards and Honors	13
10	Awards Participants	13
11	Appendix.....	13

1 Heading

PI: Peng Yin

Organization: Harvard University

ONR Award Number: N00014-14-1-0610 & N00014-16-1-2182

Award Title: Scaling up complexity of DNA brick structures

2 Scientific and Technical Objectives

The objective of our work under this grant was to develop methodologies for building highly complex structures using synthetic DNA strands. *In vitro*, we focused on greatly expanding the size and utility of structures created with our “DNA Brick” motif [Nature 2012 and Science 2012], as well as developing new methodologies for small or Origami-based structures. We then sought to apply these and other structures to the organization of other matter such as gold or carbon.

We also focused on dynamic complexity, with the objective of applying DNA nanotechnology to the complex, parallel tasks of *in vivo* translational regulation, the conditional generation of new DNA species, and imaging applications.

3 Approach

We report herein on the following approaches:

Development of **fundamental molecular mechanisms** that enable the assembly of complex DNA nanostructures, both structural and dynamic, both *in vitro* and *in vivo*.

Development of **transformative, real-world applications** based on shape-controlled nanostructures applied to the electronics industry, complex regulation of cellular protein production, and super-resolution and multiplexed imaging.

4 Concise Accomplishments

Work proceeded in three broad topics, as follows. References in parentheses refer to publications listed in Section 9.1.

Novel structure generation, expansion, and application. We describe a simple and robust method to construct large, fully addressable, three-dimensional structures by using short strands called DNA bricks. Structures reached 1 GDa in total molecular weight, incorporating 10,000 unique components – a 100-fold advance in size that was recently published in Nature (3). We further expanded on this DNA Brick technology to create repeating DNA “crystals,” (9) high-yield, micron-scale, 2D thin films with prescribed, sub-10 nm 3D features, and in turn used them to self-assemble carbon nanotubes in regular arrays (1). These structures were analyzed in part using our novel sequencing approach (5). Also demonstrated were two other new forms of structure, a particularly compact cube structure of synthetic DNA (7) and a new methodology for creating DNA or RNA single-stranded origami (2). Finally, we demonstrated the conversion of DNA into programmable, carbonized structures (6), the casting of gold nanoparticles from DNA structure “foundries” (8), and the use of DNA as masks for nanoscale lithography (4).

DNA-based synthetic biology. Control and assembly of structures *in vivo* marks a significant increase in difficulty. We have reported a strategy for RNA-based nanodevices that can exert programmatic control over mRNA translation. The range of these devices encompasses a set of 100 or more orthogonal signals (14) that can be organized into an unprecedented variety of functions with little crosstalk. We applied this to demonstrate complex logic evaluation in living bacterial cells (12). *In vitro*, we developed the “Auto-cycling Proximity Recording” mechanism to continuously create DNA “records” of protein or other molecular proximity, and used it to measure

and reconstruct 7-point geometries (11). We further expanded this conditional DNA assembly in a variety of “Primer Exchange Reactions” (10). Finally, we integrated our and other computational tools into a web-based portal for dynamic DNA circuit design (13).

Imaging technologies and applications. We expanded our DNA PAINT method of super-resolution microscopy to 3D structure determination (17), as well as developed a method of dramatically expanding the multiplexing capability of super- or normal-resolution microscopy to 10 or more “colors” (signal types) (14), and further demonstrated the utility of this in complex tissue samples (15).

5 Expanded Accomplishments

The following descriptions are expansions of the above, placed in the order of Section 9.1.

5.1 Novel structure generation, expansion, and application

5.1.1 High-precision scaling of ultra-dense carbon nanotube arrays at 2-nm resolution.

The pursuit of high-performance, energy-efficient computation requires the continuous miniaturization of FETs (field-effect transistors), and the International Technology Roadmap of Semiconductors (ITRS) projects the scaling of the multi-channel FETs from the current 14-nm technology node to a 5-nm technology node before year 2025. Over the past 20 years, carbon nanotubes (CNT) have been widely considered a promising channel material to replace Si at these scales due to high current capacity at low operation voltage, but challenges in programming the inter-CNT pitches (center- to-center spacing between two adjacent nano-channels) of parallel CNT arrays had to be overcome. Traditional thin-film-based deposition methods and directional growth generally yield CNTs in irregular-spaced bundles or with wide orientation distributions. We report the scaling of inter-CNT pitch using a method called Spatially Hindered Integration of Nanowire Electronics (SHINE). Specifically, we refine and apply our DNA brick crystal technology to self-assemble micron-scale 2D thin films with prescribed sub-10 nm 3D features. These scales represent features an order of magnitude more narrow than those made through conventional lithography for confining CNT deposition. We then apply these DNA bricks to spatially confine the directional deposition of CNTs. Further mediating CNT deposition with DNA hybridization, we constructed parallel CNT arrays with uniform programmable pitches ranging between 24.1 nm and 10.4 nm at the assembly yield over 95%. Structures were expanded into millimeter-scale arrays using lithographically defined grooves on silicon substrate to spatially confine the placement orientation of the CNT-decorated DNA brick crystals. Finally, as a proof of concept, we constructed a dual-channel CNT FET with uniformly prescribed pitch at 24 nm, using a complementary metal–oxide–semiconductor (CMOS) compatible process. For the first time, SHINE enables 2-nm spatial resolution and sub-2 nm precision for programming inter-CNT pitch over millimeter scale, which meet the fabrication requirements for multi-channel CNT FETs at 5-nm technology node and beyond. More generally, SHINE could possibly enable a strategy to arrange diverse 1D nanomaterials into large scale functional devices to enable future high-performance energy-efficient nano-electronics in post-Si era, and may further allow integration strategies compatible with and complementary to current photolithography and block-copolymer schemes.

5.1.2 Single-stranded DNA and RNA Origami.

Self-folding of an information-carrying polymer into a compact particle with defined structure and function (e.g. folding of a peptide into a protein) is foundational to biology and offers attractive potential as a synthetic strategy. Although multi-component self-assembly has produced complex synthetic nucleic acids nanostructures, uni-molecular folding only sees limited progress. We have described a framework to design and synthesize a single DNA or RNA strand that efficiently self-folds into a prescribed complex, knot-free structure, termed single-stranded DNA or RNA origami

(ssOrigami). The generality of the method was validated by the construction of 18 multi-kilobase DNA and 5 RNA ssOrigami, including a ~10,000 nt DNA structure (~40 times larger than previous largest discrete single-stranded DNA nanostructure) and a ~6,000 nt RNA structure (~10 times larger than previous largest RNA structure). The space filling nature of ssOrigami permitted the experimental construction of programmable patterns of markers (e.g. a 'smiley' face) and cargoes on its surface, its single-strandedness enabled the demonstration of facile replication of the strand *in vitro* and in living cells, and its programmability allowed us to codify the design process and develop a web-based automated design tool. The work establishes that unimolecular folding, similar to multi-component self-assembly, is a fundamental, general, and practically tractable strategy for constructing complex and replicable nucleic acids nanostructures, and expands the design space and material scalability for bottom-up nanotechnology.

5.1.3 Programmable Self-Assembly of Three-Dimensional Nanostructures from 10,000 Unique Components.

DNA self-assembly provides an effective "bottom-up" approach for producing complex user-prescribed nanostructures. In 2006, DNA origami brought bottom-up nanotechnology from kilodalton scale to megadalton scale by enabling practical construction of fully addressable megadalton-size nanostructures (typically 5 megadalton using an M13 virus scaffold, composed of 200 unique strands totaling 15,000 nucleotides). Using a new DNA brick motif, we report here the design and practical construction of gigadalton-size nanostructures using commercially available, unpurified, short DNA strands through simple one-pot isothermal reaction. A fully-addressable 0.5 gigadalton cuboid (100 times larger and more complex than DNA origami) was designed using newly-developed 'Nanobricks' 3D editing software and self-assembled from over 30,000 unique components (i.e. DNA strands). It contains 1.7 million nucleotides, comparable to the entire genome of simple bacteria. We also demonstrate the one-pot assembly of a 1 gigadalton tetramer cuboid composed of four identical 262-megadalton cuboid monomers. Further, we used a 125 megadalton cuboid to serve as a canvas for self-assembling structures with complex cavities including a bear, bunny, helicoid, and showing three different projections. A new, sequencing-based structure analysis methodology was then used to demonstrate that the bear structure had a 98% strand incorporation rate despite its size and complexity. DNA bricks thus help bring bottom-up nanotechnology and synthetic molecular self-assembly from megadalton scale to gigadalton scale by enabling the construction of complex discrete 3D gigadalton nanostructures with user-specified dimensions and shapes.

5.1.4 DNA nanostructures-mediated molecular imprinting lithography.

This paper describes the fabrication of polymer stamps using DNA nanostructure templates. This process creates stamps having diverse nanoscale features with dimensions ranging from several tens of nanometers to micrometers. DNA nanostructures including DNA nanotubes, stretched λ -DNA, two-dimensional (2D) DNA brick crystals with three-dimensional (3D) features, hexagonal DNA 2D arrays, and triangular DNA origami were used as master templates to transfer patterns to poly(methyl methacrylate) and poly(L-lactic acid) with high fidelity. The resulting polymer stamps were used as molds to transfer the pattern to acryloxy perfluoropolyether polymer. This work establishes an approach to using self-assembled DNA templates for applications in soft lithography. Barcode extension for analysis and reconstruction of structures.

5.1.5 Programmably-shaped carbon nanostructure from shape-conserving carbonization of DNA.

DNA nanostructures are versatile templates for low cost, high resolution nanofabrication. However, due to the limited chemical stability of pure DNA structures, their applications in nanofabrication have long been limited to low temperature processes or solution phase reactions. Here, we demonstrate the use of DNA nanostructure as a template for high temperature, solid-

state chemistries. We show that programmably shaped carbon nanostructures can be obtained by a shape-conserving carbonization of DNA nanostructures. The DNA nanostructures were first coated with a thin film of Al_2O_3 by atomic layer deposition (ALD), after which the DNA nanostructure was carbonized in low pressure H_2 atmosphere at 800–1000 °C. Raman spectroscopy and atomic force microscopy (AFM) data showed that carbon nanostructures were produced and the shape of the DNA nanostructure was preserved. Conductive AFM measurement shows that the carbon nanostructures are electrically conductive.

5.1.6 A compact DNA cube with side length 10 nm.

A small and compact DNA cube with zeptoliter volume is constructed by means of a generalized DNA brick concept using short synthetic oligonucleotides with varying lengths. By mimicking design principles from the DNA origami technique, the DNA cube offers higher stability and assembly yields compared to other approaches. Its potential application as nanoscale fluorescent probe is demonstrated using super-resolution imaging.

5.1.7 Casting inorganic structures with DNA molds.

We report a general strategy for designing and synthesizing inorganic nanostructures with arbitrarily prescribed three-dimensional shapes. Computationally designed DNA strands self-assemble into a stiff “nanomold” that contains a user-specified three-dimensional cavity and encloses a nucleating gold “seed.” Under mild conditions, this seed grows into a larger cast structure that fills and thus replicates the cavity. We synthesized a variety of nanoparticles with 3-nanometer resolution: three distinct silver cuboids with three independently tunable dimensions, silver and gold nanoparticles with diverse cross sections, and composite structures with homo- and heterogeneous components. The designer equilateral silver triangular and spherical nanoparticles exhibited plasmonic properties consistent with electromagnetism-based simulations. Our framework is generalizable to more complex geometries and diverse inorganic materials, offering a range of applications in biosensing, photonics, and nanoelectronics.

5.1.8 DNA brick crystals with prescribed depths.

The ability to assemble functional materials with precise spatial arrangements is important for applications ranging from protein crystallography to photovoltaics. Here, we describe a general framework for constructing two-dimensional crystals with prescribed depths and sophisticated three-dimensional features. The crystals are self-assembled from single-stranded DNA components called DNA bricks. We demonstrate the experimental construction of DNA brick crystals that can grow to micrometre size in their lateral dimensions with precisely controlled depths up to 80 nm. They can be designed to pack DNA helices at angles parallel or perpendicular to the plane of the crystal and to display user-specified sophisticated three-dimensional nanoscale features, such as continuous or discontinuous cavities and channels.

5.2 DNA-based synthetic biology

5.2.1 Programmable autonomous synthesis of single-stranded DNA.

DNA performs diverse functional roles in biology, nanotechnology and biotechnology, but current methods for autonomously synthesizing arbitrary single-stranded DNA are limited. Here, we introduce the concept of primer exchange reaction (PER) cascades, which grow nascent single-stranded DNA with user-specified sequences following prescribed reaction pathways. PER synthesis happens in a programmable, autonomous, in situ and environmentally responsive fashion, providing a platform for engineering molecular circuits and devices with a wide range of sensing, monitoring, recording, signal-processing and actuation capabilities. We experimentally demonstrate a nanodevice that transduces the detection of a trigger RNA into the production of a DNzyme that degrades an independent RNA substrate, a signal amplifier that conditionally

synthesizes long fluorescent strands only in the presence of a particular RNA signal, molecular computing circuits that evaluate logic (AND, OR, NOT) combinations of RNA inputs, and a temporal molecular event recorder that records in the PER transcript the order in which distinct RNA inputs are sequentially detected.

5.2.2 A DNA nanoscope via auto-cycling proximity recording.

Analysis of the spatial arrangement of molecular features enables the engineering of synthetic nanostructures and the understanding of natural ones. The ability to acquire a comprehensive set of pairwise proximities between components would satisfy an increasing interest in investigating individual macromolecules and their interactions, but current biochemical techniques detect only a single proximity partner per probe. Here, we present a biochemical DNA nanoscopy method that records nanostructure features in situ and in detail for later readout. Based on a conceptually novel auto-cycling proximity recording (APR) mechanism, it continuously and repeatedly produces proximity records of any nearby pairs of DNA-barcoded probes, at physiological temperature, without altering the probes themselves. We demonstrate the production of dozens of records per probe, decode the spatial arrangements of 7 unique probes in a homogeneous sample, and repeatedly sample the same probes in different states.

5.2.3 Complex cellular logic computation using ribocomputing devices.

Synthetic biology aims to develop engineering-driven approaches to program cellular function that could yield transformative technologies. Synthetic gene circuits that combine DNA, protein, and RNA components have demonstrated a range of functions including bistability, oscillation, feedback, and logic capabilities. However, scaling up these circuits remains challenging due to the limited number of designable, orthogonal, high-performance parts, the empirical and often tedious composition rules, and substantial resource requirements for encoding and operation. Here, we report a strategy for constructing RNA-only nanodevices to evaluate complex logic in living cells. Such 'ribocomputing' systems are composed of de-novo-designed parts and operate via predictable and designable base-pairing rules, allowing for effective in silico design of computing devices with prescribed configurations and functions in complex cellular environments. These devices operate at the post-transcriptional level and use an extended RNA transcript to co-localize all circuit sensing, computation, signal transduction, and output elements in the same self-assembled molecular complex, which reduces diffusion-mediated signal losses, lowers metabolic cost, and improves circuit reliability. We demonstrate that ribocomputing devices in *E. coli* can evaluate two-input logic with dynamic range up to 900-fold. Successful operation of ribocomputing devices based on programmable RNA interactions suggests that systems employing the same design principles could be implemented in other host organisms or in extracellular settings.

5.2.4 DyNAMiC Workbench: an integrated development environment for dynamic DNA nanotechnology.

Dynamic DNA nanotechnology provides a promising avenue for implementing sophisticated assembly processes, mechanical behaviours, sensing and computation at the nanoscale. However, design of these systems is complex and error-prone, because the need to control the kinetic pathway of a system greatly increases the number of design constraints and possible failure modes for the system. Previous tools have automated some parts of the design workflow, but an integrated solution is lacking. Here, we present software implementing a three 'tier' design process: a high-level visual programming language is used to describe systems, a molecular compiler builds a DNA implementation and nucleotide sequences are generated and optimized. Additionally, our software includes tools for analysing and 'debugging' the designs in silico, and for importing/exporting designs to other commonly used software systems. The software we present is built on many existing pieces of software, but is integrated into a single package—

accessible using a Web-based interface at <http://molecular-systems.net/workbench>. We hope that the deep integration between tools and the flexibility of this design process will lead to better experimental results, fewer experimental design iterations and the development of more complex DNA nanosystems.

5.2.5 Toehold switches: de-novo-designed regulators of gene expression.

Efforts to construct synthetic networks in living cells have been hindered by the limited number of regulatory components that provide wide dynamic range and low crosstalk. Here, we report a class of de-novo-designed prokaryotic riboregulators called toehold switches that activate gene expression in response to cognate RNAs with arbitrary sequences. Toehold switches provide a high level of orthogonality and can be forward engineered to provide average dynamic range above 400. We show that switches can be integrated into the genome to regulate endogenous genes and use them as sensors that respond to endogenous RNAs. We exploit the orthogonality of toehold switches to regulate 12 genes independently and to construct a genetic circuit that evaluates 4-input AND logic. Toehold switches, with their wide dynamic range, orthogonality, and programmability, represent a versatile and powerful platform for regulation of translation, offering diverse applications in molecular biology, synthetic biology, and biotechnology. Imaging technologies and applications

5.3 Imaging technologies and applications

5.3.1 Rapid sequential in situ multiplexing with DNA-Exchange-Imaging in Neuronal Cells and Tissues.

To decipher the molecular mechanisms of biological function, it is critical to map the molecular composition of individual cells or even more importantly tissue samples in the context of their biological environment in situ. Immunofluorescence (IF) provides specific labeling for molecular profiling. However, conventional IF methods have finite multiplexing capabilities due to spectral overlap of the fluorophores. Various sequential imaging methods have been developed to circumvent this spectral limit but are not widely adopted due to the common limitation of requiring multirounds of slow (typically over 2 h at room temperature to overnight at 4 °C in practice) immunostaining. We present here a practical and robust method, which we call DNA Exchange Imaging (DEI), for rapid in situ spectrally unlimited multiplexing. This technique overcomes speed restrictions by allowing for single-round immunostaining with DNA-barcoded antibodies, followed by rapid (less than 10 min) buffer exchange of fluorophore-bearing DNA imager strands. The programmability of DEI allows us to apply it to diverse microscopy platforms (with Exchange Confocal, Exchange-SIM, Exchange-STED, and Exchange-PAINT demonstrated here) at multiple desired resolution scales (from ~300 nm down to sub-20 nm). We optimized and validated the use of DEI in complex biological samples, including primary neuron cultures and tissue sections. These results collectively suggest DNA exchange as a versatile, practical platform for rapid, highly multiplexed in situ imaging, potentially enabling new applications ranging from basic science, to drug discovery, and to clinical pathology.

5.3.2 DNA-barcoded labeling probes for highly multiplexed Exchange-PAINT imaging.

Recent advances in super-resolution fluorescence imaging allow researchers to overcome the classical diffraction limit of light, and are already starting to make an impact in biology. However, a key challenge for traditional super-resolution methods is their limited multiplexing capability, which prevents a systematic understanding of multi-protein interactions on the nanoscale. Exchange-PAINT, a recently developed DNA-based multiplexing approach, in theory facilitates spectrally-unlimited multiplexing by sequentially imaging target molecules using orthogonal dye-labeled 'imager' strands. While this approach holds great promise for the bioimaging community, its widespread application has been hampered by the availability of DNA-conjugated ligands for

protein labeling. Herein, we report a universal approach for the creation of DNA-barcoded labeling probes for highly multiplexed Exchange-PAINT imaging, using a variety of affinity reagents such as primary and secondary antibodies, nanobodies, and small molecule binders. Furthermore, we extend the availability of orthogonal imager strands for Exchange-PAINT to over 50 and assay their orthogonality in a novel DNA origami-based crosstalk assay. Using our optimized conjugation and labeling strategies, we demonstrate nine-color super-resolution imaging in situ in fixed cells.

5.3.3 Polyhedra self-assembled from DNA tripods and characterized with 3D DNA-PAINT.

DNA self-assembly has produced diverse synthetic three-dimensional polyhedra. These structures typically have a molecular weight no greater than 5 megadaltons. We report a simple, general strategy for one-step self-assembly of wireframe DNA polyhedra that are more massive than most previous structures. A stiff three-arm-junction DNA origami tile motif with precisely controlled angles and arm lengths was used for hierarchical assembly of polyhedra. We experimentally constructed a tetrahedron (20 megadaltons), a triangular prism (30 megadaltons), a cube (40 megadaltons), a pentagonal prism (50 megadaltons), and a hexagonal prism (60 megadaltons) with edge widths of 100 nanometers. The structures were visualized by means of transmission electron microscopy and three-dimensional DNA-PAINT super-resolution fluorescent microscopy of single molecules in solution.

6 Major problems / Issues

None.

7 Technology Transfer

See Sections 9.4. (Patents) and 9.5 (Start-ups).

8 Foreign Collaborations and Supported Foreign Nationals

Foreign Nationals: Dongran Han, Rizal Hariadi, Juanita Lara, Hiroshi Sasaki, Nicolas Garreau de Loubresse, Di Liu, Wei Sun, Jie Shen, Weidong Xu

Foreign Collaborations: N/A

9 Productivity

9.1 Refereed Journal Articles

9.1.1 Structures

1. W. Sun, Z. Zhao, J. Shen, N. Arellano, C. Rettner, J. Tang, T. Cao, Z. Zhou, T. Ta, W.M. Shih, H.T. Maune, and P. Yin, High-precision scaling of ultra-dense carbon nanotube arrays at 2-nm positioning resolution. in preparation.
2. D. Han, X. Qi, C. Myhrvold, B. Wang, M. Dai, S. Jiang, M. Bates, Y. Liu, B. An, F. Zhang, H. Yan and P. Yin, Single-stranded DNA and RNA Origami. *Science*, accepted (2017)
3. L.L. Ong, N. Hanikel, O.K. Yaghi, C. Grun, M.T. Strauss, P. Bron, J. Lai-Kee-Him, et al. Programmable Self-Assembly of Three-Dimensional Nanostructures from 10,000 Unique Components. *Nature* 552:7683 (2017)
4. C. Tian, H. Kim, W. Sun, Y. Kim, P. Yin, and H. Liu, DNA nanostructures-mediated molecular imprinting lithography, *ACS Nano* 11:1 (2017)

5. C. Myhrvold, M. Baym, N. Hanikel, L. L. Ong, J. S. Gootenberg and P. Yin, Barcode extension for analysis and reconstruction of structures. *Nature Communications* 8: 14698 (2017)
6. F. Zhou, W. Sun, K. B. Ricardo, D. Wang, J. Shen, P. Yin, and H. Liu. Programmably-shaped carbon nanostructure from shape-conserving carbonization of DNA *ACS Nano* 10:3 (2016)
7. M. B. Scheible, L. L. Ong, J. B. Woehrstein, R. Jungmann, P. Yin and F. C. Simmel, A compact DNA cube with side length 10 nm. *Small* 11:39 (2015)
8. W. Sun, E. Boulais, Y. Hakobyan, W. Wang, A. Guan, M. Bathe, P. Yin, Casting inorganic structures with DNA molds, *Science* 346:1258361 (2014)
9. Y. Ke, L.L. Ong, W. Sun, J. Song, M. Dong, W.M. Shih, P. Yin, DNA brick crystals with prescribed depths, *Nature Chemistry* 6:994-1002 (2014)

9.1.2 Synthetic Biology

10. J. Kishi, T.E. Schaus, N. Gopalkrishnan, F. Xuan, and P. Yin, Programmable autonomous synthesis of single-stranded DNA, *Nature Chemistry* (2017)
11. T.E. Schaus, S. Woo, F. Xuan, X. Chen and P. Yin, A DNA nanoscope via auto-cycling proximity recording, *Nature Communications* 8:696 (2017)
12. A.A. Green, J. Kim, D. Ma, P.A. Silver, J. J. Collins and P. Yin, Complex cellular logic computation using ribocomputing devices. *Nature* 548:7665 (2017)
13. C. Grun, J. Werfel, D.Y. Zhang, and P. Yin, DyNAMiC Workbench: an integrated development environment for dynamic DNA nanotechnology, *J. R. Soc. Interface* 12: 20150580 (2015)
14. A.A. Green, P.A. Silver, J.J. Collins, P. Yin, Toehold switches: de-novo-designed regulators of gene expression, *Cell* 159:925-939 (2014)

9.1.3 Imaging

15. Y. Wang, J.B. Woehrstein, N. Donoghue, M. Dai, M. S. Avendano, R.C.J. Schackmann, J. Zoeller, S.S.H. Wang, P.W. Tillberg, D. Park, S.W. Lapan, E.S. Boyden, J.S. Brugge, P.S. Kaeser, G.M. Church, S.S. Agasti, R. Jungmann, P. Yin, Rapid sequential in situ multiplexing with DNA-Exchange-Imaging in Neuronal Cells and Tissues, *Nano Letters* 17:10 (2017)
16. S.S. Agasti, Y. Wang, F. Schueder, A. Sukumar, R. Jungmann and P. Yin DNA-barcoded labeling probes for highly multiplexed Exchange-PAINT imaging *Chem. Sci.* 8:4 (2017)
17. R. Iinuma, Y. Ke, R. Jungmann, T. Schlichthaerle, J.B. Woehrstein, P. Yin, Polyhedra self-assembled from DNA tripods and characterized with 3D DNA-PAINT, *Science* 344:65-69 (2014)

9.2 Non-Refereed Journal Articles

None.

9.3 Workshops and Conferences

1. International Workshop on DNA-based Nanotechnology (dnatec17), May 29, 2017, Dresden, Germany

2. Gordon Research Conference on "Self-Assembly and Supramolecular Chemistry", May 21st, 2017, Les Diablerets, Switzerland.
3. The second ISH symposium - Applications of In Situ Hybridisation in Research and Disease, Cambridge, UK, May 17th, 2017.
4. Department of Biomedical Engineering, Tufts University, Feb. 6th, 2017.
5. Elkin Lecture, Emory University, Dec. 2nd, 2016.
6. Center for Molecular Bioengineering, TU Dresden, Nov. 21st, 2016.
7. Advances in Cell Engineering, Imaging and Screening, a VIB Tools and Technologies Conference, Leuven, Belgium, Nov. 17th, 2016.
8. RNA Nanotechnology Conference, Berkshire, United Kingdom, Aug. 2nd, 2016.
9. The Fourth Annual Workshop on Micro- and Nanotechnologies in Medicine, Cambridge, MA, July 26th, 2016.
10. Gordon Research Conference on "Single Molecule Approaches to Biology", Hong Kong, July 3rd, 2016.
11. Sino-US Synthetic Biology Workshop, Guangzhou, China, July 1st, 2016.
12. 7th international symposium on Bioanalysis, Biomedical Engineering and Nanotechnology (ISBBN 2016), Changsha, China, May 27th, 2016.
13. 3rd Materials Beyond Symposium, Shanghai, China, May 26th, 2016.
14. Worcester annual nanotech symposium (NanoWorcester), Worcester, MA, Apr. 14th, 2016.
15. Workshop on 10 years of DNA origami, Pasadena, CA, March 14th, 2016.
16. Biophysical Society 60th Annual Meeting, Los Angeles, CA, Feb. 27th, 2016.
17. Department of Bioengineering, Rice University, Houston, TX, Feb. 9th, 2016.
18. Amgen, Inc., Cambridge, MA, Nov. 10th, 2015.
19. Molecular Foundry, Lawrence Berkeley National Laboratory, Berkeley, CA, Nov. 3rd, 2015.
20. Tenth International Meeting of Institute for Translational Medicine and Therapeutics at Penn, Pennsylvania, PA, Oct. 11th, 2015.
21. Physical Sciences Symposia-2015 on Quantum Science Symposium and Crystal/Graphene, 2015
22. Science Symposium, Cambridge, MA, Sep. 22, 2015
23. 2nd ACM International Conference on Nanoscale Computing and Communication, Boston, MA, September. 21st, 2015 [Keynote].
24. DARPA Workshop on Transient Materials, Arlington, VA, Sep. 2nd, 2015.
25. The Second Blavatnik Science Symposium, New York City, NY, Aug. 6th, 2015.
26. The Eleventh International Fab Lab Conference (Fab11), Boston, MA, Aug. 5th, 2015.

27. The Third Annual Workshop on Micro- and Nanotechnologies in Medicine, Cambridge, MA, July 28th, 2015.
28. Gordon Conference on Nucleosides, Nucleotides and Oligonucleotides, Newport, RI, July 1st, 2015.
29. Gordon Conference on Synthetic Biology, Newry, ME, June 30th, 2015.
30. Albany 2015: The 19th Conversation, Albany, NY, June 11th, 2015.
31. ECI Conference on Photonics for Biology, Medicine and Surgery, Vail, CO, June, 7th, 2015.
32. 1st Synthetic Biology Young Scholar Forum (SynBioYSF), Beijing, May 23rd, 2015 [Keynote].
33. College of Chemistry and Molecular Engineering, Beijing, May 22nd, 2015.
34. Yale Chemical Biology Symposium, New Haven, CT, May, 15th, 2015.
35. Department of Materials Science and Engineering, Northwestern University, Evanston, IL, May 12, 2015

9.4 Translation: Patents

SECTION 1 - SUBJECT INVENTIONS N00014-16-1-2182 and N00014-14-1-0610						
5. "SUBJECT INVENTION"						
NAMES OF INVENTORS (a)	TITLE OF INVENTION (b)	DISCLOSURE NUMBER, PATENT APPLICATION NUMBER, OR PATENT NUMBER (c)	Election to File Patent Application			
			(1) US		(2) Foreign	
			(a) Yes	(b) No	(a) Yes	(b) No
Yin, Peng; Woehrstein, Johannes; Strauss, Maximilian T.; Jungmann, Ralf	Metafluorophores	5557		X		X
Yin, Peng; Schaus, Thomas; Chen, Xi	APR: Auto-Cyclic Proximity Recording	15/542,953	X		X	
Yin, Peng; Ong, Luvena L.; Simmel, Friedrich; Scheible, Max Boy	Compact DNA Cubes	5973		X		X
Yin, Peng; Jungmann, Ralf; Ong, Luvena L.; Zhang, David Yu; Wei, Diming (Bryan)	Triggeered Assembly of Metafluorophores	15/622,261	X		X	
Yin, Peng; Kishi, Jocelyn; Schaus, Thomas; Xuan, Feng; Gopalkrishnan, Nikhil; Woo, Sungwook	Primer exchange reactions (PER)	6173		X		X
Yin, Peng; Han, Dongran	Automated design of arbitrary 3D DNA nanostructures with high spatial precision	6182		X		X
Yin, Peng; Beliveau, Brian J.; Kishi, Jocelyn	Probe Miner: A rapid, genome-scale oligo FISH probe discovery pipeline	6218		X		X
Yin, Peng; Schaus, Thomas; Gopalkrishnan, Nikhil	Sequence design for efficient assembly of nucleic acid structures	6286		X		X
Yin, Peng; Xuan, Feng; Dai, Mingjie; Chen, Xi	Conditional Primer Extension for Single-Molecule Protein Detection	6369		X		X
Yin, Peng; Kishi, Jocelyn; Xuan, Feng	Primer Exchange Reactions (PER) for Isothermal PCR	6371		X		X
Yin, Peng; Kishi, Jocelyn; Kim, Jongmin; Strassmann, Steve; Schaus, Thomas	Molecular Verification Systems for Enhanced Identification and Secure Access Control	6544		X		X
Yin, Peng; Myhrvold, Cameron; Baym, Michael Hartmann	Brick Improvement	6554		X		X
Yin, Peng; Jungmann, Ralf; Woehrstein, Johannes B.; Agasti, Sarit S.; Wang, Yu	Highly Multiplexed Diffraction-Limited and Super-Resolution Imaging Using DNA-Exchange-Imaging	6684		X		X
Yin, Peng; Wang, Yu; Jungmann, Ralf; Agasti, Sarit S.	DNA-Protein conjugation and purification for DNA-Exchange-Imaging	6687		X		X
Yin, Peng; Kishi, Jocelyn; Beliveau, Brian J.; Saka, Sinem Kirti; Wang, Yu	PER Amplification for Imaging	6704		X		X

9.5 Translation: Start-ups

The PI, Peng Yin, has recently co-founded two companies based in part on this work. Both are backed by leading venture capital companies:

1. **Ultivue:** High-definition multiplex imaging, based in part on Dr. Yin's PAINT and Exchange-PAINT technologies. See: www.ultivue.com
2. **NuProbe:** Rare genetic allele detection, based in part on Dr. Yin's DNA-based toehold probe systems. See: www.nuprobe.com

9.6 Awards and Honors

1. World Economic Forum Young Scientist Award, 2015. Press: <https://agenda.weforum.org/news/world-economic-forum-honours-its-2015-young-scientists-community-at-annual-meeting-of-the-new-champions/>
2. Blavatnik National Awards for Young Scientists, Finalist, 2015. Press: <http://www.prnewswire.com/news-releases/blavatnik-national-awards-for-young-scientists-announce-2015-finalists-300087851.html>
3. World Economic Forum Young Scientist Award, 2014. Press: <http://www.weforum.org/news/world-economic-forum-honours-its-2014-young-scientists-community-annualmeeting-new-champions>
4. Inaugural ACS Synthetic Biology Young Scientist Award, 2014. Press: <http://wyss.harvard.edu/viewpage/540/>
5. Blavatnik National Awards for Young Scientists, Finalist, 2014. Press: <http://blavatnikawards.org/news/items/blavatnik-national-awards-announce-30-finalists/>
6. NIH Transformative Research Award, 2013. Press: <http://wyss.harvard.edu/viewPressrelease/126/15>
7. NSF Expedition in Computing Award, 2013. Press: http://www.nsf.gov/news/news_summ.jsp?cntn_id=128886

10 Awards Participants

Military Personnel: N/A

Salary Support: Peng Yin, Jie Shen, Dongran Han, Hiroshi Sasaki, Nicolas Garreau de Loubresse, Di Liu, Erik Hernandez, Weidong Xu, Ninning Liu, Thomas Schaus, Rizal Hariadi, Luvera Ong, Juanita Lara, Wei Sun, Casey Grun, Anita Chandrahas, Maier Avendano, Mingjie Dai, and Christina Chen.

11 Appendix

Pre-prints of publication #1, not yet published, and links to Yin lab website, where all other publications are available as pdfs.

<https://yin.hms.harvard.edu/publications.html>

High-precision scaling of ultra-dense carbon nanotube arrays at 2-nm positioning resolution

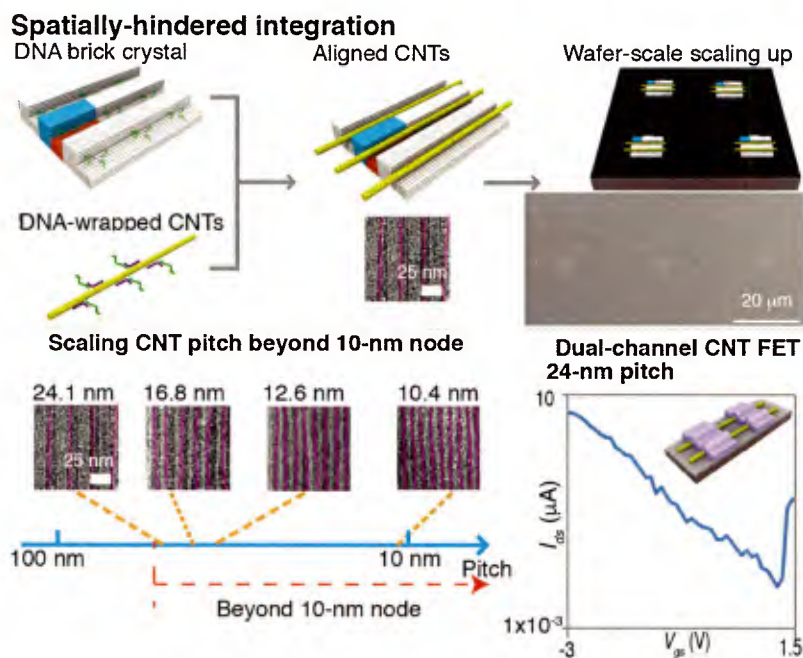
Wei Sun^{1,2†} Zhao Zhao^{2,3,4†} Jie Shen^{1,2†} Noel Arellano⁵ Charles Rettner⁵ Jianshi Tang⁶ Tianyang Cao⁷ Zhiyu Zhou⁷ Toan Ta⁶ Shu-Jen Han⁶
Willam M. Shi^{2,3,4} Hareem T. Maune^{*5} Peng Yin^{*1,2}

Department of Systems Biology, Harvard Medical School, Boston, Massachusetts 02115¹,
Wyss Institute for Biologically Inspired Engineering, Harvard University, Boston, Massachusetts 02115²
Department of Cancer Biology, Dana-Farber Cancer Institute, Harvard Medical School, Boston, Massachusetts 02115³
Department of Biological Chemistry and Molecular Pharmacology, Harvard Medical School, Boston, Massachusetts 02115⁴
IBM Almaden Research Center, San Jose, California 95120⁵
IBM Thomas J. Watson Research Center, Yorktown Heights, New York 10598⁶
Department of Chemistry, Tsinghua University, Beijing 100084, China⁷

[†] These authors contributed equally to this work

E-mail address*: py@hms.harvard.edu; hmaune@us.ibm.com

Abstract. Since the invention of first carbon nanotube (CNT) field-effect transistor (FET) twenty years ago, it has been one of the long pursued goals to scale the multi-channel CNT FETs beyond the 5-nm technology node. Traditional thin-film-based de-position methods and directional growth generally yield CNTs in irregular-spaced bundles or with wide orientation distributions. Therefore, the resolution and precision of inter-CNT pitch, the key parameters defining the lateral CNT spacing, still fail to meet the requirements for constructing high-performance FETs specified in the International Technology Roadmap for Semiconductors (ITRS). We report the scaling of inter-CNT pitch using a method called Spatially Hindered Integration of Nanowire Electronics (SHINE). Specifically, by using nano-trenches on micron-scale DNA brick crystals to spatially confine the directional deposition of CNT mediated by DNA hybridization, we constructed parallel CNT arrays with uniform programmable pitches ranging between 24.1 nm and 10.4 nm at the assembly yield over 95%. Furthermore, we assembled them into millimeter-scale arrays using lithographically defined grooves on silicon substrate to spatially confine the placement orientation of the CNT-decorated DNA brick crystals. Finally, as a proof of concept, we constructed a dual-channel CNT FETs with uniformly prescribed pitch at 24 nm, using a complementary metaloxidesemiconductor (CMOS) compatible process. For the first time, SHINE enables 2-nm spatial resolution and sub-2 nm precision for programming inter-CNT pitch over millimeter scale, which meet the fabrication requirements for multi-channel CNT FETs at sub-5 nm node. More generally, SHINE could possibly enable a strategy to arrange diverse one-dimensional nanomaterials into large scale functional devices to enable future high-performance energy-efficient nano-electronics in post-Si era, and may further allow integration strategies compatible with and complementary to current photographically and block-copolymer schemes.



Summary Figure : SHINE: Spatially Hindered Integration of Nanowire Electronics. Top, integration of CNTs onto the DNA brick crystals and their hierarchical assembly over millimeter-scale area on silicon substrates. Bottom left, demonstration of uniform inter-CNT pitch (24.1 nm, 16.8 nm, 12.6 nm, and 10.4 nm) compatible with 5-nm and beyond technology node. Bottom right, dual-channel CNT FET at 24 nm pitch.

Introduction.

The pursuit for high-performance energy-efficient computation requires the continuous scaling of FET (field-effect transistor). International Technology Roadmap of Semiconductors (ITRS) projects the scaling of the multi-channel FETs from current 14-nm technology node¹ to 5-nm technology node before year 2025.² Over the past 20 years, carbon nanotube (CNT) has been widely considered as a promising channel material to replace Si at sub-5 nm technology node, owing to its high current-capacity at low operation voltage and ballistic transport.³⁻⁵ To achieve the projected technology node for multi-channel CNT FET, it is necessary to program the inter-CNT pitches (center-to-center spacing between two adjacent nano-channels) of parallel CNT arrays with both high spatial resolution to maximize the on current and high precision to minimize pitch variation.^{6,7}

However, the difficulties in controlling the orientation and placement of individual CNTs present challenges for the fabrication resolution/precision through traditional thin-film techniques^{5,6,8}. Different orientations of neighboring CNTs produce variable inter-CNT pitches from end-to-end.^{9,10} The sliding of CNTs relative to one another during deposition, as well as CNT aggregation, also yield irregularly spaced CNT bundles¹¹⁻¹³ at identical CNT orientations. Even for CNTs deposited within nano-trenches around 60–200 nm wide,^{14,15} such challenges still remain. As a result, unlike lithography-defined Si Fin-FETs with both sub-50 nm consistent fin pitch from end-to-end and pitch variation less than 5 nm,¹ pitch variation in existing high-density CNT arrays are often observed larger than the averaged pitch value,¹⁰ thus does not meet the fabrication requirements for scaling multi-channel FET at 14 nm technology node and beyond^{6,8}. Alternatively, CNT arrays assembled using double-stranded DNA linkers exhibit nanoscale tunable inter-CNT pitch,¹⁶ but only contain a small number of CNTs (2.4 on average, less than the typical requirement of 6 CNTs per FET⁶). Importantly, the technique lacks control over the placement of CNT arrays on large scale, which is necessary for constructing integrated circuits.

Densely aligned narrow nano-trenches could provide a promising route for scaling the inter-CNT pitch towards the sub-5 nm technology nodes.⁷ Sufficiently narrow trenches could precisely confine the orientation of individual embedded CNTs and prevent the aggregation of CNTs within the trench. However, considering the small diameter of CNT ($\sim 1 - 2$ nm) and the required inter-CNT pitch (25 nm and smaller depending on the contact resistance)⁷, large-scale fabrication of ultra-dense nano-trenches requires sub-5 nm fabrication resolution, which is difficult for conventional lithography. Recent developments in structural DNA nanotechnology, in particular DNA origami¹⁷⁻²⁰ and DNA bricks^{21,22}, provide alternative bottom-up strategies for constructing 3D objects at 2-nm spatial resolution. DNA brick crystals²³ further provide micron-scale 2D thin films with prescribed sub-10 nm 3D features. Hence, DNA brick crystal could provide a promising route for constructing nano-trenches that are one order of magnitude narrower than those made through conventional lithography for confining CNT deposition.^{14,15}

Using nano-trenches constructed on the micron-scale DNA brick crystals to spatially confine the directional deposition of CNTs, we report a method called Spatially Hindered Integra-

tion of Nanowire Electronics (SHINE) for scaling the inter-CNT pitch (Fig. 1). Specifically, DNA nano-trenches confine the orientation of individual CNTs along the longitudinal axis of the nano-trenches. DNA hybridization between the single-stranded handles within nano-trenches and the anti-handles on CNTs mediates the CNT deposition and compensates for the entropy loss during the deposition. Meanwhile, DNA brick crystals provide the templates for assembling CNTs with micron-scale width ($0.1 \mu\text{m} \sim 0.4 \mu\text{m}$). By programming the DNA trench periodicity, we successfully scale the inter-CNT pitch in the assembled CNT arrays ranging from 24.1 nm to 10.4 nm, at the assembly yield over 95%. Under the optimized design, SHINE enables 2-nm spatial resolution and sub-2 nm precision for programming inter-CNT pitch. The self-assembly nature of SHINE enables the parallel assembly of millions of CNTs onto DNA brick crystals at uniform inter-CNT pitch. Furthermore, by using lithographically defined grooves on silicon substrate to spatially confine the placement orientation of the CNT-decorated DNA brick crystals, we assembled them into millimeter-scale arrays. Finally, as a proof of concept, we demonstrate CNT FET devices, including a dual-channel CNT-FETs, with uniformly prescribed 24 nm inter-CNT pitch through a CMOS (complementary metaloxide semiconductor)-compatible DNA removal and device fabrication method.

In the future, enabled by SHINE, multi-channel CNT FETs could be potentially massively assembled at sub-10 nm inter-CNT pitch over wafer-scale. Other 1D nanomaterials, including inorganic nanowires,²⁴ graphene nanoribbons²⁵ and semiconducting polymers,²⁶ could also be integrated into similar multi-channel FET using DNA brick crystals as templates. And the channel pitch of the assembled multi-channel devices could be scaled to address the performance metrics beyond the 5 nm technology node projected by ITRS.² Besides the parallel arrays demonstrated here, 3D crossbar architectures or vertically aligned arrays could be potentially constructed by designing templates with intersecting nano-trenches or vertical tunnels. More generally, SHINE could possibly enable a strategy to arrange diverse one-dimensional nanomaterials into large scale functional devices to enable future high-performance energy-efficient nano-electronics in post-Si era, and may further allow integration strategies compatible with and complementary to current photographically and block-copolymer schemes.

CNT arrays with 24-nm inter-CNT pitch

Design overview. Fig. 1 illustrates the general process for SHINE. We first design and assemble a DNA brick crystal template with parallel nano-trenches. Within each trench, multiple single-stranded DNA (ssDNA) handles project out of the bottom layer. Meanwhile, using a two-step assembly method, we wrap CNT surface with ssDNA anti-handles (sequence complementary to the DNA handles) through non-covalent interactions. At mild conditions, the hybridization between the ssDNA handles within the DNA nano-trenches and the anti-handles on CNTs mediates the CNT deposition into the DNA nano-trenches and produces parallel CNT arrays at prescribed inter-CNT pitch.

Design details.

Next we describe the design and experimental details for the

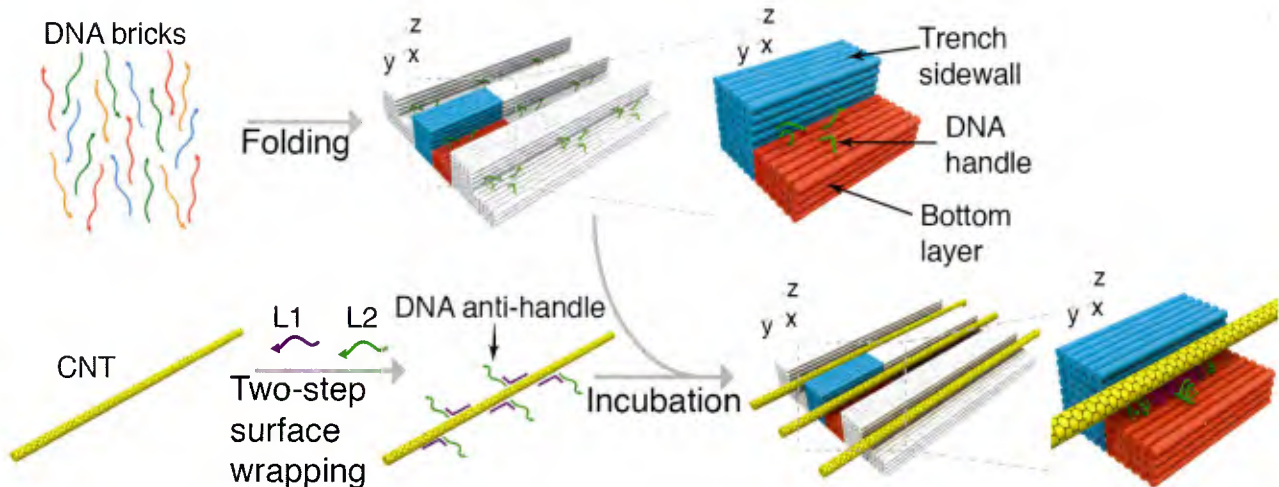


Figure 1: Design schematic for SHINE. The blue and orange colored bundles represent a repeating unit of designed DNA brick crystals. Specifically, the blue bundles are the sidewalls of DNA nano-trench; and the orange bundles are the bottom layer of DNA nano-trench. Green curves denote the DNA handles. The yellow rod represents the CNTs.

above process. For a DNA brick crystal with 25-nm periodicity along x direction, we used a repeating unit cell of 6,768 base-pairs. Within each unit cell (Fig. 1), the sidewall of DNA nano-trench consisted of 6 helices \times 8 helices \times 94 basepairs (the designed dimensions of 12.6 nm \times 16.8 nm \times 33 nm) along x - y - z directions; and the bottom layer of the nano-trench was composed of 6 helices \times 4 helices \times 94 basepairs (the designed dimensions of 12.6 nm \times 8.4 nm \times 33 nm) along x - y - z direction. At the top surface of the bottom layer, we introduced four 14-nucleotide (nt) ssDNA handles by extending the 3' or 5' ends of four selected DNA bricks. Extending the repeating unit along the x - z directions yielded the micron-scale DNA brick crystals with parallel nano-trenches (Fig. 2A)

We used a two-step assembly method²⁷ to introduce DNA anti-handles (sequence complementary to the DNA handles within DNA nano-trenches) onto CNTs (Fig. S2 in Supplementary Sect. S2.2). First, CNT surface was wrapped with two-domain single-stranded DNA L1, which contained a wrapping domain of repeating GT sequence at 3' end and a 16-nt binding domain at 5' end to hybridize with L2. Wrapping CNT with ssDNA used non-covalent π - π stacking between DNA nucleotides and the CNT surface. Next, a two-domain single-stranded DNA L2 was introduced to hybridize with L1-wrapped CNTs. Within L2, a 16-nt binding domain was introduced at 5' end for hybridizing with its complement domain in L1. And a 14-nt anti-handle domain at 3' end of L2 was designed to hybridize with the DNA handles.

Experimental implementation.

In a typical experiment, DNA brick crystals were folded via multi-staged incubation reaction. 90 μ L mixture of unpurified DNA bricks (pH 7.9, containing 300 nM of each brick, 5 mM Tris, 1 mM EDTA, and 40 mM MgCl₂ in the solution, without careful adjustment of each brick stoichiometry) were incubated at 80°C for 15 min, 44°C for 12 h, 39°C for 72 h, and 31°C for 8 h sequentially. For wrapping CNTs with ssDNAs, we mixed strand L1 with CNT powder in buffer (1 \times TBE and 100 mM NaCl at pH 8.3), and sonicated the solution for 1 h, followed by high-speed centrifuge to remove the aggregates. The super-

natant solution was purified using a 100 kD Amicon filter to get rid of excess DNA. Strand L2 was then added to the purified CNT-L1 solution and incubated at 35 °C for 2 h and 24°C for 16 h sequentially. L2-wrapped CNTs (0.4 μ L) were then mixed with 5.6 μ L diluted DNA brick crystals solution (100 \times dilution, containing 10 mM MgCl₂ and 400 mM NaCl) and incubated at 33°C for 9 h. The crude product was deposited on either glow-discharged copper grid for imaging with transmission electron microscopy (TEM) after negative staining or mica for imaging with atomic force microscopy (AFM).

Structural characterization.

TEM imaging confirmed the successful formation of the designed DNA brick crystal templates (Fig. 2B and Fig. S4 in Supplementary Sect. S5), and the confined deposition of CNT arrays within the DNA nano-trenches (Fig. 2E and Fig. S8 in Supplementary Sect. S6). Before CNT deposition, we observed alternative dark (bottom layer) – bright (sidewall) morphologies on the DNA brick crystals (zoomed-in TEM image in Fig. 2B). Each dark and bright regions exhibited identical six-layered DNA helices as designed (Fig. 2A). The assembled DNA brick crystals were single-domain structures, with measured crystal periodicity as 25.3 \pm 0.3 nm ($N = 50$ from 10 different crystals) along the x direction after dried on surface (corresponding to 2.1 nm diameter per helix for the dehydrated double-stranded DNA). DNA brick crystals exhibited wide dimension distributions and typically appeared in a leaflike morphology with longer dimension along the DNA helical direction. In the zoomed-out image in Supplementary Fig. S4C, the largest crystal exhibited dimensions around 1.3 μ m \times 200 nm in x - z directions. Surface density of the DNA brick crystal was around 1 crystal per μ m², according to TEM counting (Fig. S4B in Supplementary Sect. S5).

After CNT deposition, we found bright parallel lines appearing on the dark bottom layer exclusively, corresponding to the aligned CNTs (see design in Fig. 2D, TEM images in Fig. 2E and Fig. S8 in Supplementary Sect. S6). In the zoomed-in TEM image (Fig. 2E), the diameter of CNT was measured around 3 nm, slightly larger than the 1-2 nm diameter of unwrapped

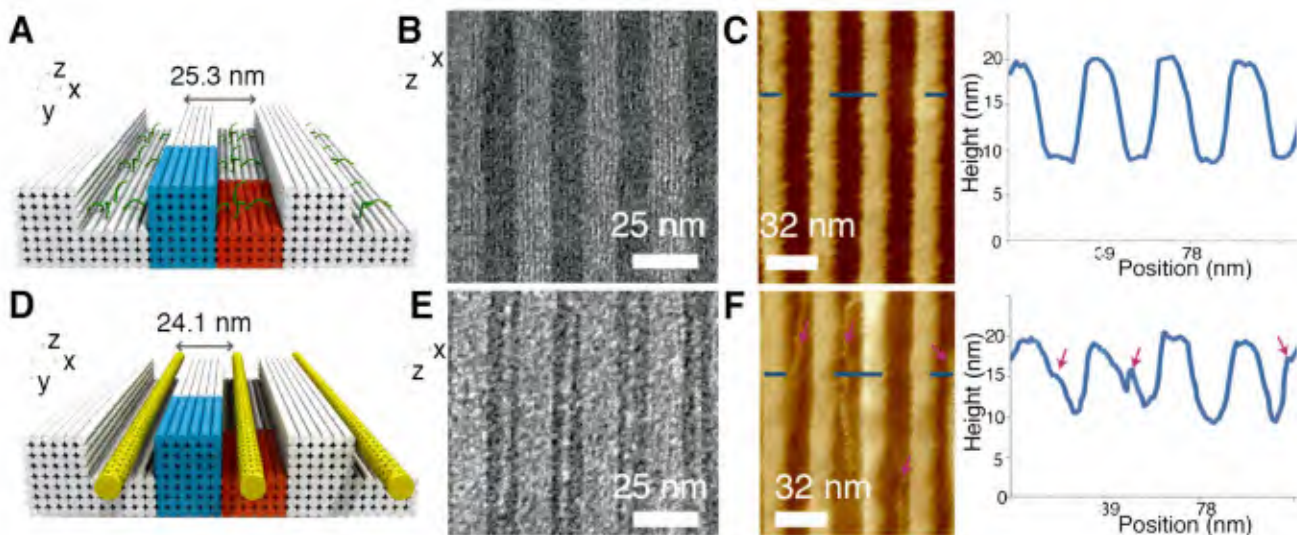


Figure 2: Assembling of CNT arrays with 24 nm inter-CNT pitch. (A) Design schematic for DNA brick crystals. The colored bundles present a repeating unit of DNA brick crystals with 25.2 nm periodicity along x direction. The blue bundles are the sidewalls of DNA nano-trench; and the orange bundles are the bottom layer of DNA nano-trench. Green curves denote the DNA handles. (B) Zoomed-in TEM image ($100 \text{ nm} \times 100 \text{ nm}$) of the DNA brick crystals along the x - z projection direction. The scale bar is 25 nm. (C) Left, liquid AFM image of the DNA brick crystals. The scale bar is 32 nm. Blue line represents the location for the height profile. Right, height profile of the DNA brick crystals. (D) Design schematic for CNT deposited on DNA brick crystals. The yellow rods represent CNTs. (E) Zoomed-in TEM image ($100 \text{ nm} \times 100 \text{ nm}$) of the CNTs deposited onto the DNA brick crystals along the x - z projection direction. The scale bar is 25 nm. (F) Left, liquid AFM image of the CNTs deposited onto the DNA brick crystals along the x - z projection direction. The scale bar is 32 nm. Blue line represents location for the height profile. Right, height profile of the CNTs patterned on the DNA brick crystals along the x - z projection direction. Pink arrows indicate the CNTs patterned on the DNA brick crystals.

CNTs, owing to the wrapping DNA layer around CNTs after staining (see TEM images for the DNA-wrapped CNTs in Fig. S3 in Supplementary Sect. S4). The measured inter-CNT pitch was $24.1 \pm 1.7 \text{ nm}$ ($N = 50$ from 10 different crystals). For every two neighboring CNTs, we measured three different positions along the longitudinal axis of CNT), similar to the x direction periodicity of the DNA brick crystal template. The range of inter-CNT pitch variation, defined as the difference between the maximum and minimum spacing values of two adjacent CNTs, was around 7.8 nm. And the percent relative range of the inter-CNT pitch, defined as the range of inter-CNT pitch divided by the averaged value of inter-CNT pitch, was calculated as 33%. In contrast, on a flat substrate, a range larger than 30 nm and a percent relative range over 140% were reported for CNT arrays with similar pitch.¹⁰ Hence, by limiting the surface rotation of CNTs with DNA nano-trench sidewall, SHINE provides higher precision for placing ultra-dense CNT arrays than flat substrate-based assembly, as evaluated by (1) the standard deviation, (2) the range value, and (3) the percent relative range of inter-CNT pitch.

Because DNA brick crystals exhibited wide dimension distribution along x - z directions, we observed variable numbers of aligned CNTs on different DNA brick crystals, ranging between 4 and 15. More than 70% of the assembled CNT arrays contained at least six CNTs. In contrast, CNT arrays assembled from double-stranded DNA linkers contain average 2.4 CNTs per array at similar inter-CNT pitch.¹⁶ We also observed end position offset for CNTs along z direction from trench to trench (Fig. S9 in Supplementary Sect. S6), due to the heterogeneous CNT length and the absence of end registration for CNTs. Notably, although the width of the DNA trench (12 nm) was larger

than the diameter of individual CNT, we did not observe multiple CNTs aligned side by side within individual trenches. We hypothesize that, because of the negative charged DNAs around CNT surface, CNTs repulsed one another. Therefore, aligning CNTs side by side within individual trenches was energetically unfavorable. The deposited CNTs also spatially shielded the remaining ssDNA handles beneath the CNTs from being accessed by other CNTs, hence preventing undesirable CNT stacking/aggregation.

The integrity of the DNA brick crystals was not affected by CNT assembly. After CNT deposition, both DNA sidewalls and bottom layer remained identical six-layered (along x direction) DNA helices as confirmed by TEM imaging (Fig. 2E). Surface density of the CNT-decorated DNA brick crystals was $0.01 \text{ crystal per } \mu\text{m}^2$ (Fig. S8B in Supplementary Sect. S6 for the large-field-of-view image), as a result of the $100\times$ dilution of the DNA brick crystals in the CNT incubation reaction solution.

CNTs were aligned along the longitudinal axis of the nano-trenches. Angular deviation, which was defined as the difference between CNT axis and the longitudinal axis of DNA nano-trenches, was less than 2° for all the deposited CNTs. Notably, the angular deviation of CNTs within nano-trenches was much smaller than previous result on flat DNA templates (less than 25% CNTs exhibit angular deviation less than 5°),²⁸ demonstrating the effectiveness of SHINE in CNT alignment.

We further analyzed the assembly yield by TEM counting (Supplementary Sect. S3). Assembly yield was defined as the total inner nano-trenches occupied by the parallel CNT arrays over the total numbers of inner DNA nano-trenches. Two peripheral DNA nano-trenches on the edges were excluded considering the crystal formation on the growing edges was not accomplished.

Over 95% assembly yield was observed for 9 randomly selected DNA brick crystals with more than 45 inner trenches (Fig. S9 in Supplementary Sect. S6). Less than 5% inner nano-trenches were found not occupied by CNTs.

The aligned CNTs were also characterized by liquid AFM. In an empty trench, top surface of the bottom layer exhibited an average height of 10 nm (Fig. 2C). After CNT assembly, new peaks with heights around 15–17 nm were observed near the DNA sidewalls (around 20 nm in height, Fig. 2F). The height change (5–7 nm) of the new peaks is similar to the sum of the dsDNA handle length (3–4 nm) and CNT diameter (2–3 nm), indicating only single-layer CNT deposited within the DNA nano-trenches (Fig. S10 in Supplementary Sect. S6). The relative wider inter-CNT pitch (around 32 nm) in liquid AFM, compared with TEM images, was resulted from the large diameter of hydrated dsDNAs (2.6 nm diameter per helix in hydrated dsDNAs) in liquid condition. Under tapping mode, we also observed CNT alignment disruption by AFM tips during scanning in liquid (Fig. 2F).

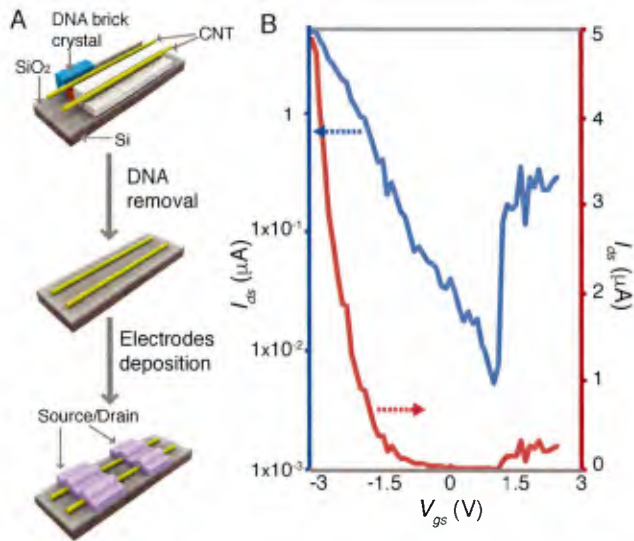


Figure 3: Constructing bottom-gated dual-channel CNT FET at 24-nm inter-CNT pitch. (A) Design schematic for DNA removal and depositing the source/drain electrodes. The blue and orange colored bundles together represent a structural repeating unit of DNA brick crystals with 24 nm periodicity along x direction. The yellow rods represent CNTs. The purple objects represent the deposited electrodes. (B) The $I_{ds}-V_{gs}$ curve plotted in both logarithmic (left axis, blue) and linear (right axis, red) scales at V_{sd} of -0.5 V for the dual-channel CNT FET.

FET construction and characterization

We have developed a CNT FET fabrication method to demonstrate viability of SHINE for nano-electronics. To construct a typical bottom-gated FET, we deposited the semiconducting CNT-decorated DNA brick crystals (24-nm inter-CNT pitch, CNT length around 300 nm, 70% purity of semiconducting CNTs) onto a Si wafer (with around 10-nm thick thermal grown surface SiO_2 , pre-cleaned with oxygen plasma, Fig. 3A top). The DNA brick crystal, DNA handles wrapped around CNTs,

and the salt residues on the substrate were gently removed through metal liftoff and controlled thermal annealing under Argon atmosphere (Fig. 3A middle, Fig. S18 in Supplementary Sect. S7). Under the optimized conditions, DNA removal did not disrupt the integrity and quality of the aligned CNTs (Fig. S19 in Supplementary Sect. S7). After DNA removal, CNTs retained 24-nm inter-CNT pitch, with less than 1-nm thick residues beneath the CNT arrays, as evidenced in AFM image (Fig. S19 in Supplementary Sect. S7). High-resolution AFM was used to register the location of the annealed CNT arrays for designing the electrodes. Finally, Ti/Pd/Au metal electrodes were fabricated using e-beam lithography for the designed CNT FET, with channel length around 40 nm (Fig. 3A bottom). Of all the devices constructed, 50% (4 out of 8) showed typical gate modulation behavior of CNT FETs. The other non-operational transistors were partially resulted from the low purity (70%) of the semiconducting CNTs used.

In general, the constructed CNT FETs (Fig. 3B and Fig. S20 in Supplementary Sect. S7) exhibited on/off current ratio of greater than 10^3 at source-to-drain bias (V_{ds}) of -0.5 V, threshold voltage around -1.5 V, and on-current density of around $100 \mu\text{A}/\mu\text{m}$. The device on-current performances were comparable to those of CNT FETs constructed from bare CNTs.^{14,15} Therefore, scaling CNT FET through SHINE does not significantly degrade the transport properties of individual CNTs. Similar to other devices using SiO_2 as dielectric layer,^{9,15} current CNT FET exhibited subthreshold swing much larger than 100 mV/dec. A typical constructed dual-channel CNT FET (Fig. 3B) exhibited on-current around $2.5 \mu\text{A}/\text{tube}$, resistance around $0.2 \text{M}\Omega/\text{tube}$, and a peak transconductance value around $66 \mu\text{S}/\mu\text{m}$. In contrast, at similar transconductance, CNT FET with closely packed CNTs (inter-CNT pitch around 2 nm) exhibited on-current around $0.1 \mu\text{A}/\text{tube} - 0.25 \mu\text{A}/\text{tube}$ and resistance around $6 \text{M}\Omega/\text{tube}$.⁹

The device performance could be further improved by using CNT arrays at a narrower inter-CNT pitch at 10 nm, longer metal-CNT contact length,⁴ higher purity of semiconducting CNTs (> 99%), cleaner contact interface (without residual PMMA, amorphous carbon or other salts), and optimized contact compositions (e.g. using Mo electrode instead of current Ti/Pd/Au electrodes).²⁹ The subthreshold swing could also be improved by replacing SiO_2 with HfO_2 as dielectric layer. To fully assess the device performance at scaled inter-CNT pitch, more multi-channel CNT FETs constructed through SHINE need to be evaluated.

Millimeter-scale integration

CNT-decorated DNA brick crystals were further deposited within the lithographically defined PMMA (polymethyl methacrylate) grooves on Si substrate, demonstrating the millimeter-scale (0.1 mm) integration of the arrays (Fig. 4). We used e-beam lithography to create periodic rectangular PMMA grooves on a flat Si substrate (Fig. 4A, left). Each groove was $2.5 \mu\text{m} \times 100 \text{nm} \times 300 \text{nm}$ along $x-y-z$ directions (Fig. S22 in Supplementary Sect. S8). The periodicity of PMMA grooves were $4 \mu\text{m} \times 1.6 \mu\text{m}$ along $x-z$ directions. The rectangular PMMA groove was designed with a length-to-width aspect ratio of 8.3 to enable the orientation control over the crystal de-

position. Within a microfluidic chamber, the solution of CNT-decorated DNA brick crystal slowly flew across the entire lithographically defined patterns. During this process, the DNA brick crystals diffused into the PMMA grooves (Fig. 4A, middle). Si substrate was then dried, followed by PMMA liftoff, leaving only the deposited brick crystals on the flat Si substrate (Fig. 4A, right). Finally, we coated the substrate with Pt and imaged the sample with SEM.

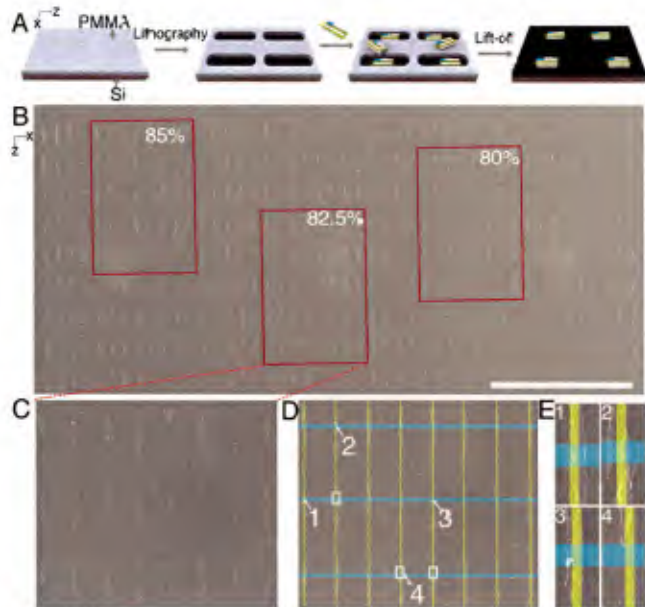


Figure 4: Millimeter-scale integration of CNT-decorated DNA brick crystals. (A) Design schematic for the hierarchically integration of CNT-decorated DNA brick crystals on Si substrate. From left to right, spin-coating of a PMMA layer onto Si wafer, e-beam lithography to create PMMA grooves, depositing CNT-decorated DNA brick crystals into the PMMA grooves, and liftoff to remove PMMA layer. (B) Zoomed-out SEM image of the deposited CNT-decorated DNA brick crystals on Si wafer after liftoff. The scale bar is 20 μm . The red rectangular circles indicate the selected DNA brick crystals for the intersection analysis. Each region contains 40 intersections. The numbers labeled in the upper right of the red rectangular circle are the occupation yield by single-layer DNA brick crystals. (C) Zoomed-in SEM image of the deposited CNT-decorated DNA brick crystals. (D) Intersection analysis for the zoomed-in SEM image in C. Each blue bar is 300-nm wide, and each yellow bar is 120-nm wide. The white circles indicate the defects at the cross section. White numbers denote the positions for the examples of occupied intersections and defects in E. (E) Typical examples of occupied intersections (examples 1-3) and defect (example 4). White numbers at the upper left corner of each panel denote the position of sample intersection in D.

Over an area of $100 \mu\text{m} \times 50 \mu\text{m}$, we created more than 500 PMMA grooves (surface density $\sim 10^7$ grooves/cm²). After liftoff of PMMA, 54.5% of the initial groove sites were occupied by the DNA brick crystals (zoomed-in and zoomed-out SEM image in Fig. 4B and C, respectively). The angular distribution, which was defined as the difference between the longitudinal axis of DNA brick crystals and the z direction of the substrate, was 37% within $\pm 1^\circ$ and 81% within $\pm 7^\circ$, according to the SEM counting of all the DNA brick crystals deposited

on Si substrate. Due to wide variation in DNA brick crystal dimensions, we observed the end position offset when depositing small DNA brick crystals (e.g. crystal shorter than 1 μm) within the PMMA grooves (Fig. S9 in Supplementary Sect. S6). Occasionally, multiple small DNA brick crystals deposited within a single PMMA groove.

To register multiple deposited DNA brick crystals in parallel, we applied an intersection analysis. Each intersection (crossed by blue and yellow bars in Fig. 4D and E) was 300 nm \times 120 nm in x - z directions (similar dimensions to the dual-channel CNT FET above), and placed periodically over Si wafer. If at least 50% area of one intersection was occupied by only a single DNA brick crystal, the intersection was labelled as occupied. Otherwise, the intersection was labelled as a defect. A defect may be generated from either multiple DNA brick crystals occupied the same intersection or less than 50% of the intersection was occupied by a single crystal. Analysis of three selected regions containing 120 intersections revealed more than 80% of the intersections occupied by the deposited DNA brick crystals (Fig. 4B). In a typical zoomed-in SEM image, we observed three defects out of twenty-four cross-sections (Fig. 4C and D). Typical examples of occupied intersections (examples 1-3) and defect (example 4) were shown in Fig. 4E. Because the DNA nano-trenches and CNTs were covered by Pt, we found weak imaging contrast within the nano-trenches and cannot differentiate CNTs from the bottom DNA layer. Millimeter-scale alignment of the CNT decorated DNA brick crystals may avoid the time-consuming registration of the CNT arrays with AFM, thus enabling future scalable fabrication of CNT FET as well as further integration of the deposited CNT FETs into complicated circuits.

Programming inter-CNT pitch

By programming DNA brick crystals with different trench periodicity along the x direction, we further demonstrated the rational scaling of inter-CNT pitch at 16.8 nm, 12.6 nm, and 10.4 nm (Fig. 5), respectively.

Within each unit cell of the narrow-pitch DNA brick crystals, we used 2 helices \times 8 helices \times 94 basepairs for the nano-trenches sidewall (Fig. 5A-C, top left); while in the bottom layer of the nano-trenches, 6 helices \times 4 helices \times 94 basepairs, 4 helices \times 4 helices \times 94 basepairs, and 3 helices \times 4 helices \times 94 basepairs were used for designed nano-trench periodicity of 16.8 nm, 12.6 nm, and 10.5 nm, respectively.

The folding condition of the narrow-pitch DNA brick crystals was identical to that of DNA brick crystal with 25-nm periodicity. After folding, DNA brick crystals exhibited measured trench periodicity of 16.8 \pm 0.4 nm, 12.7 \pm 0.2 nm, and 10.6 \pm 0.1 nm ($N = 50$ from 10 individual crystals for each design) along x direction (Fig. 5A-C, bottom left). Notably, we observed slightly twisted DNA trench sidewalls after dried in vacuum, which might be ascribed to the relative small structural stiffness of the narrow trench sidewall (containing two-layer DNA helices in the width direction). However, the average periodicity was not affected by the twisting of the DNA sidewalls. Different crystal designs showed similar surface density, around 1 crystal per μm^2 , and representative maximal crystal dimensions around 1.5 $\mu\text{m} \times 300$ nm along in x - z direction (Fig. S5, Fig. S6, and

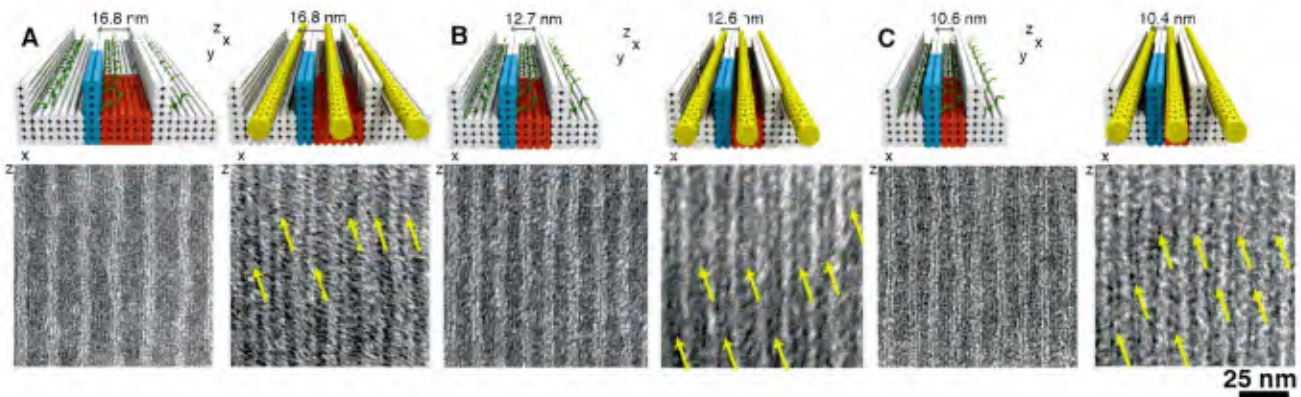


Figure 5: Programming inter-CNT pitch with DNA brick crystals. (A to C) Design (top row) and TEM images (bottom row) of programming CNT arrays with 16.8 nm **A**, 12.6 nm **B**, and 10.4 nm **C** pitches using DNA brick crystals. Within each panel, top left is the design of DNA brick crystal template. The colored bundles present a repeating unit of DNA brick crystals with selected nm periodicity along x direction. The blue bundles are the sidewalls of DNA nano-trenches; and the orange bundles are the bottom layer of DNA nano-trenches. Green curves denote the DNA handles. Top right is the design schematic CNTs patterned on DNA brick crystals. The yellow rods represent CNTs. Bottom left is the zoomed-in TEM image ($100 \text{ nm} \times 100 \text{ nm}$) of the DNA brick crystals along the x - z projection direction. Bottom right is the zoomed-in TEM image ($100 \text{ nm} \times 100 \text{ nm}$) of the CNTs assembled on DNA brick crystals along the x - z projection direction. The yellow arrows indicate the decorated CNTs. The scale bar is 25 nm.

Fig. S7 in Supplementary Sect. S5).

After CNT deposition, parallel CNTs were aligned within the DNA nano-trenches (designs in Fig. 5A-C, top right; zoomed-in TEM images in Fig. 5A-C, bottom right). The inter-CNT pitches varied from $16.8 \pm 1.5 \text{ nm}$, $12.6 \pm 0.6 \text{ nm}$, to $10.4 \pm 0.4 \text{ nm}$ ($N = 50$ from 10 individual crystals for each design). For every two neighboring CNTs, we measured three different positions along the longitudinal axis of CNT, similar to the measured periodicities in the corresponding DNA brick crystal templates, respectively. The range and the percent relative range of the inter-CNT pitch variation were characterized as 5.9 nm and 36%, 2.7 nm and 24%, 1.9 nm and 18% for 16.8 nm, 12.6 nm, and 10.4 nm inter-CNT pitches respectively. In the zoomed-out TEM images, the CNT array densities were counted around 0.01 crystal per μm^2 (Fig. S11, Fig. S13, and Fig. S15 in Supplementary Sect. S6). The angular deviation were measured less than 2° (Fig. S12, Fig. S14, and Fig. S16 in Supplementary Sect. S6).

Under the optimized CNT assembly conditions, the assembly yields were over 95% (Fig. S12, Fig. S14, and Fig. S16 in Supplementary Sect. S6), even for narrow trenches, despite the high electrostatic repulsion between negative charged DNA trench sidewalls and CNTs at narrow inter-CNT pitches. In addition, low stiffness of DNA peaks (as evidenced by the local twist of the DNA nano-trench sidewalls) did not affect the yield of CNT alignment. Narrower DNA nano-trench improves the precision for CNT alignment. When the width of DNA nano-trench was decreased to around 6 nm (in 10.4-nm pitch CNT arrays), the range of inter-CNT pitch was decreased to less than 2 nm, compared with the 5.9-nm range value in DNA nano-trench with 12-nm width (in 16.8-nm pitches CNT arrays).

Discussion

Based on the 2-nm spatial positioning resolution on micron-scale DNA brick crystals, SHINE enables a simple and scalable method towards the high-resolution scaling of ultra-dense CNT arrays for post-Si electronics. *Simplicity.* Using nano-trenches

to spatially confine the directional deposition of CNTs mediated by DNA hybridization, the difficult challenge for controlling the consistent inter-CNT pitch and orientation of millions of individual CNTs is simplified to fabricating periodic DNA nano-trenches on DNA brick crystals. By merely changing the sequence design of DNA handles, CNTs with selective chirality (e.g. metallic [Fig. 2E] or semiconducting [Fig. S19 in Supplementary Sect. S7]) can be placed at pre-designed positions in a highly reproducible manner. And the DNA hybridization-mediated CNT deposition is independent of CNT length (200 nm to $1 \mu\text{m}$) or environmental parameters (e.g. humidity or solvent flow speed in typical thin-film depositions). CNT-decorated DNA brick crystals aligned on millimeter-scale Si substrates may further simplify the batch fabrication of source/drain electrodes into parallel fabrication processes¹⁴ without the time-consuming sequential registration for each CNT array. *Scalability.* The assembly yield for CNTs within the DNA nano-trenches is higher than 95%. A $4 \mu\text{L}$ -solution at sub-10 pM crystal concentration could provide millions of assembled CNT arrays at uniform inter-CNT pitches. And the CNT-decorated DNA brick crystals could be aligned over millimeter scale. Most of the DNA brick crystals exhibit maximum width wider than 150 nm. Therefore, the majority of the assembled CNT arrays on DNA brick crystals (>70%) contain more than six CNTs per array, which is important for constructing the high-performance CNT FETs;⁶ whereas, using double-stranded DNA or DNA origami as linkers, the assembled CNT arrays contain 2~3 CNTs per array on average,^{16,30} and are difficult to align over large scale. *High-resolution pitch scaling.* Through SHINE, prescribed inter-CNT pitch could be uniformly scaled from 24.1 nm to 10.4 nm, and potentially down to 6 nm, based on the 2-nm spatial positioning resolution of DNA bricks²³ and the high-precision CNT alignment within narrow nano-trenches. Sub-2 nm positioning precision for inter-CNT pitch could be comparable to the fabrication precision through lithography.^{6,8} Therefore, SHINE provides the precise programmability on inter-CNT pitch and meets the fabrication requirement for CNT FETs at 5-nm tech-

nology node⁷ and beyond. In contrast, using traditional thin-film deposition methods, uniform CNT arrays exhibit either large uniform inter-CNT pitches^{14,15} (>100 nm) or wider inter-CNT pitch distribution¹⁰ than current Si Fin-FETs.^{6,8} Similar to the Moore's law-governed pitch scaling from 60 nm (22-nm node, Intel)³¹ to 42 nm (14-nm node, Intel)¹ in Si Fin-FETs, SHINE provides around 30% smaller inter-CNT pitch from 24.1 nm to 16.8 nm and from 16.8 nm to 12.6 nm. The orientation of individual CNTs could be reliably manipulated at high resolution, with angular distribution less than 2°.

SHINE builds a bridge between the diverse synthetic library of 1D non-Si nanomaterials and the high-performance energy-efficient chips^{13,32–34} at 10-nm channel pitch. Besides CNT demonstrated here, other 1D nanomaterials, including inorganic nanowires,²⁴ graphene nanoribbons²⁵ and semiconducting polymers,²⁶ may also be confined within the DNA nano-trenches. Not limited to current parallel arrays, 3D crossbar architectures or vertical aligned arrays could also be constructed at 10-nm channel pitch by designing DNA brick crystals with intersecting nano-trenches or vertical tunnels.

Although SHINE is initially demonstrated using DNA brick crystals, the technical foundations for SHINE, spatial confinement at single-CNT resolution and binding-stabilized nanowire deposition within nano-trenches, are generalizable beyond DNA self-assembly. Transferring the 3D geometric information from DNA nanostructures to inorganic substrates, such as SiO₂,^{35,36} may provide inorganic nano-trenches with sub-5 nm width for positioning individual CNTs. Besides DNA hybridization, chemical interactions, such as π - π stacking and electrostatic interactions,^{9,37} or physical forces, such as directional electric field,^{38,39} may also be used to compensate the entropy loss during nanowire integration.

Towards future CNT logic technology at 10-nm inter-CNT pitch, several challenges still need to be addressed in current DNA brick crystal-based SHINE. First, because current 2D DNA brick crystals extend repetitively along the x - z directions, we observed uneven crystal width and therefore non-uniform number of CNTs along the x -direction. Second, the absence of spatial confinement along the z -direction produces the end position offset for CNT alignment. Third, the wide distributions of crystal dimensions result in relative large angular deviation during millimeter-scale alignment. To address these challenges, it is essential to provide 2D spatial confinement for CNT positioning and improve the control over size variation for both DNA templates and CNTs. Using discrete DNA brick structures with prescribed 3D dimensions²² as templates, CNT arrays could be assembled with identical CNT numbers on each DNA structure template. Meanwhile, PMMA grooves could be manufactured with exact dimensions to fit the mono-dispersed DNA structures. Hence the orientation freedom of DNA templates on substrate will be minimized. Closed end trenches that fit the length-sorted CNTs are key to reducing the positioning offset for CNTs. Once fully immobilized within the closed end trenches, the end-position of the length-sorted CNTs will be registered to the trench ends, providing the confined alignment of CNTs in both x and z directions. The assembled multi-channel CNT FETs may thus have identical CNT components and device parameters (e.g. contact length and channel length) to minimize

transistor-to-transistor variations.

Although SHINE is initially demonstrated using DNA brick crystals, the technical foundations for SHINE, spatial confinement at single-CNT resolution and binding-stabilized nanowire deposition within nano-trenches, are generalizable beyond DNA self-assembly. Transferring the 3D geometric information from DNA nanostructures to inorganic substrates, such as SiO₂,^{35,36} may provide inorganic nano-trenches with sub-5 nm width for positioning individual CNTs. Besides DNA hybridization, chemical interactions, such as π - π stacking and electrostatic interactions,^{9,37} or physical forces, such as directional electric field,^{38,39} may also be used to compensate the entropy loss during nanowire integration.

Bottom-up assembly of CNT arrays through SHINE provides inter-CNT pitches down to 10 nm and atomic-precise channel edge. Together with the lithographically defined sub-10-nm channel length^{40,41} and contact length,²⁹ as well as defect-tolerant algorithm for operating CNT FETs,¹³ it may be potentially possible to construct future high-performance electronics from energy-efficient multi-channel CNT FETs at 5-nm technology node and beyond^{2,7}.

References

1. S. Natarajan, M. Agostinelli, S. Akbar, M. Bost, A. Bowonder, V. Chikarmane, S. Chouksey, A. Dasgupta, K. Fischer, Q. Fu, T. Ghani, M. Giles, S. Govindaraju, R. Grover, W. Han, D. Hanken, E. Haralson, M. Haran, M. Heckscher, R. Heussner, P. Jain, R. James, R. Jhaveri, I. Jin, H. Kam, E. Karl, C. Kenyon, M. Liu, Y. Luo, R. Mehandru, S. Morarka, L. Neiberg, P. Packan, A. Paliwal, C. Parker, P. Patel, R. Patel, C. Pelto, L. Pipes, P. Plekhanov, M. Prince, S. Rajamani, J. Sandford, B. Sell, S. Sivakumar, P. Smith, B. Song, K. Tone, T. Troeger, J. Viedemer, M. Yang, and K. Zhang. A 14 nm logic technology featuring 2nd-generation FinFET, air-gapped interconnects, self-aligned double patterning and a 0.0588 μm^2 sram cell size. *Electron Dev. Meeting (IEDM)*, pages 3–7, 2014.
2. The international technology roadmap for semiconductors: 2013.
3. A. Javey, J. Guo, Q. Wang, M. Lundstrom, and H. Dai. Room-temperature transistor based on a single carbon nanotube. *Nature*, 424:654–657, 2003.
4. A. D. Franklin and Z. Chen. Length scaling of carbon nanotube transistors. *Nature Nanotech.*, 5:858–862, 2010.
5. A. D. Franklin. Nanomaterials in transistors: From high-performance to thin-film applications. *Science*, 349:aab2750, 2015.
6. G. S. Tulevski, A. D. Franklin, D. Frank, J. M. Lobe, Q. Cao, H. Park, A. Afzali, S.-J. Han, J. B. Hannon, and W. Haensch. Toward high-performance digital logic technology with carbon nanotubes. *ACS Nano*, 8:8730–8745, 2014.
7. C.-S. Lee, E. Pop, A. D. Franklin, W. Haensch, and H.-S. P. Wong. A compact virtual-source model for carbon nanotube fets in the sub-10-nm regime part ii: Extrinsic elements, performance assessment, and design optimization. *Electron Devices, IEEE Transactions on*, 62(9):3070–3078, 2015.
8. M. F. L. De Volder, S. H. Tawfik, R. H. Baughman and A. J. Hart. Carbon nanotubes: Present and future commercial applications. *Science*, 339:535–539, 2013.
9. Q. Cao, S.-J. Han, G. S. Tulevski, Y. Zhu, D. D. Li, and Haensch W. Arrays of single-walled carbon nanotubes with full surface coverage for high-performance electronics. *Nature Nanotech.*, 8:180–186, 2013.
10. Q. Cao, S.-J. Han, and G. S. Tulevski. Fringing-field dielectrophoretic assembly of ultrahigh-density semiconducting nanotube arrays with a self-limited pitch. *Nature Commun.*, 5:5071, 2014.
11. S. J. Kang, C. Kocabas, T. Ozel, M. Shim, N. Pimparkar, M. A. Alam, S. V. Rotkin, and J. A. Rogers. High-performance electronics using dense, perfectly aligned arrays of single-walled carbon nanotubes. *Nature Nanotech.*, 2:230–236, 2007.
12. M. M. Shulaker, H. Wei, N. Patil, J. Provine, H.-Y. Chen, H.-S. P. Wong, and S. Mitra. Linear increases in carbon nanotube density through multiple transfer technique. *Nano Lett.*, 11:1881–1886, 2011.

13. M. M. Shulaker, G. Hills, N. Patil, H. Wei, H.-Y. Chen, H.-S. P. Wong, and S. Mitra. Carbon nanotube computer. *Nature*, 501:526–530, 2013.
14. H. Park, A. Afzali, S.-J. Han, G. S. Tulevski, A. D. Franklin, J. Tersoff, J. B. Hannon, and W. Haensch. High-density integration of carbon nanotubes via chemical self-assembly. *Nature Nanotech.*, 7:787–791, 2012.
15. J. Wu, A. Antaris, M. Gong, and H. Dai. Top-down patterning and self-assembly for regular arrays of semiconducting single-walled carbon nanotubes. *Adv. Mater.*, 26:6151–6156, 2014.
16. S.-P. Han, H. T. Maune, R. D. Barish, M. Bockrath, and W. A. Goddard, III. DNA-linker-induced surface assembly of ultra dense parallel single walled carbon nanotube arrays. *Nano Lett.*, 12:1129–1135, 2012.
17. P. W. K. Rothmund. Folding DNA to create nanoscale shapes and patterns. *Nature*, 440:297–302, 2006.
18. S. M. Douglas, H. Dietz, T. Liedl, B. Hogberg, F. Graf, and W. M. Shih. Self-assembly of DNA into nanoscale three-dimensional shapes. *Nature*, 459:414–418, 2009.
19. H. Dietz, S. M. Douglas, and W. M. Shih. Folding DNA into twisted and curved nanoscale shapes. *Science*, 325:725–730, 2009.
20. D. R. Han, S. Pal, J. Nangreave, Z. T. Deng, Y. Liu, and H. Yan. DNA origami with complex curvatures in three-dimensional space. *Science*, 332:342–346, 2011.
21. B. Wei, M. J. Dai, and P. Yin. Complex shapes self-assembled from single-stranded DNA tiles. *Nature*, 485:623–626, 2012.
22. Y. G. Ke, L. L. Ong, W. M. Shih, and P. Yin. Three-dimensional structures self-assembled from DNA bricks. *Science*, 338:1177–1183, 2012.
23. Y. Ke, L. L. Ong, W. Sun, J. Song, M. Dong, W. M. Shih, and P. Yin. DNA brick crystals with prescribed depths. *Nature Chem.*, 6:994–1002, 2014.
24. Z. Deng, S. Pal, A. Samanta, H. Yan, and Y. Liu. DNA functionalization of colloidal II–VI semiconductor nanowires. *Chem. Sci.*, 3:2234–2240, 2013.
25. J. Cai, P. Ruffieux, R. Jaafar, M. Bieri, T. Braun, S. Blankenburg, M. Muoth, A. P. Seitsonen, M. Saleh, X. Feng, K. Mullen, and R. Fasel. Atomically precise bottom-up fabrication of graphene nanoribbons. *Nature*, 466:470–473, 2010.
26. J. B. Knudsen, L. Liu, A. L. B. Kodal, M. Madsen, Q. Li, J. Song, J. B. Woehrstein, S. F. J. Wickham, M. T. Strauss, F. Schueder, J. Vinther, A. Krissanaprasit, D. Gudnason, A. A. A. Smith, R. Ogaki, A. N. Zelikin, F. Besenbacher, V. Birkedal, P. Yin, W. M. Shih, R. Jungmann, M. Dong, and K. V. Gothelf. Routing of individual polymers in designed patterns. *Nature Nanotech.*, 10:892–898, 2015.
27. Z. Zhao, Y. Liu, and H. Yan. DNA origami templated self-assembly of discrete length single wall carbon nanotubes. *Org. Biomol. Chem.*, pages 596–598, 2013.
28. H. T. Maune, S. P. Han, R. D. Barish, M. Bockrath, W. A. Goddard III, P. W. K. Rothmund, and E. Winfree. Self-assembly of carbon nanotubes into two-dimensional geometries using DNA origami templates. *Nature Nanotech.*, 5:61–66, 2010.
29. Q. Cao, S.-J. Han, J. Tersoff, A. D. Franklin, Y. Zhu, Z. Zhang, G. S. Tulevski, J. Tang, and W. Haensch. End-bonded contacts for carbon nanotube transistors with low, size-independent resistance. *Science*, 350:68–72, 2015.
30. A. Mangalum, M. Rahman, and M. L. Norton. Site-specific immobilization of single-walled carbon nanotubes onto single and one-dimensional DNA origami. *J. Am. Chem. Soc.*, 135:2451–2454, 2013.
31. C. Auth, C. Allen, A. Blattner, D. Bergstrom, M. Brazier, M. Bost, M. Buehler, V. Chikarmane, T. Ghani, T. Glassman, R. Grover, W. Han, D. Hanken, M. Hattendorf, P. Hentges, R. Heussner, J. Hicks, D. Ingerly, P. Jain, S. Jaloviar, R. James, D. Jones, J. Jopling, S. Joshi, C. Kenyon, H. Liu, R. McFadden, B. McIntyre, J. Neiryck, C. Parker, L. Pipes, I. Post, S. Pradhan, M. Prince, S. Ramey, T. Reynolds, J. Roesler, J. Sandford, J. Seiple, P. Smith, C. Thomas, D. Towner, T. Troegger, C. Weber, P. Yashar, K. Zawadzki, and K. Mistry. A 22 nm high performance and low-power CMOS technology featuring fully-depleted tri-gate transistors, self-aligned contacts and high density MIM capacitors. *Symp. VLSI Tech. Dig.*, pages 131–132, 2012.
32. Q. Cao, H.-S. Kim, N. Pimparkar, J. P. Kulkarni, C. Wang, M. Shim, K. Roy, M. A. Alam, and J. A. Rogers. Medium-scale carbon nanotube thin-film integrated circuits on flexible plastic substrates. *Nature*, 454:495–500, 2008.
33. L. Ding, Z. Zhang, S. Liang, T. Pei, S. Wang, Y. Li, W. Zhou, J. Liu, and L.-M. Peng. CMOS-based carbon nanotube pass-transistor logic integrated circuits. *Nature Commun.*, 3:677, 2012.
34. M. L. Geier, J. J. McMorrow, W. Xu, J. Zhu, C. H. Kim, T. J. Marks, and M. C. Hersam. Solution-processed carbon nanotube thin-film complementary static random access memory. *Nature Nanotech.*, 10:944–948, 2015.
35. S. P. Surwade, S. Zhao, and H. Liu. Molecular lithography through DNA-mediated etching and masking of SiO₂. *J. Am. Chem. Soc.*, 133:11868–11871, 2011.
36. S. P. Surwade, F. Zhou, B. Wei, W. Sun, A. Powell, C. O'Donnell, P. Yin, and H. Liu. Nanoscale growth and patterning of inorganic oxides using DNA nanostructure templates. *J. Am. Chem. Soc.*, 135:6778–6781, 2013.
37. X. Li, L. Zhang, X. Wang, I. Shimoyama, X. Sun, W.-S. Seo, and H. Dai. Langmuir-blodgett assembly of densely aligned single-walled carbon nanotubes from bulk materials. *J. Am. Chem. Soc.*, 129:4890–4891, 2007.
38. X. Q. Chen, T. Saito, H. Yamada, and K. Matsushige. Aligning single-wall carbon nanotubes with an alternating-current electric field. *Appl. Phys. Lett.*, 78:3714–3716, 2001.
39. A. Vijayaraghavan, S. Blatt, D. Weissenberger, M. Oron-Carl, F. Hennrich, D. Gerthsen, H. Hahn, and R. Krupke. Ultra-large-scale directed assembly of single-walled carbon nanotube devices. *Nano Lett.*, 7:1556–1560, 2007.
40. A. D. Franklin, M. Luisier, S.-J. Han, G. Tulevski, C. M. Breslin, L. Gignac, M. S. Lundstrom, and W. Haensch. Sub-10 nm carbon nanotube transistor. *Nano Lett.*, 12:758–762, 2012.
41. M. M. Shulaker, J. V. Rethy, T. F. Wu, L. S. Liyanage, H. Wei, Z. Li, E. Pop, G. Gielen, H.-S. P. Wong, and S. Mitra. Carbon nanotube circuit integration up to sub-20 nm channel lengths. *ACS Nano*, 8:3434–3443, 2014.

Acknowledgments: The authors would like to thank D. Pastuszak for assistance in draft preparation. This work is supported by DARPA Young Faculty Award N66001-11-1-4136, ONR Young Investigator Program Award N000141110914, NSF CAREER Award CCF1054898, NIH Director's New Innovator Award 1DP2OD007292 and Wyss Institute Faculty Startup Fund to P.Y.